JOURNAL OF GEOPHYSICAL RESEARCH, VOL. 105, NO. A8, PAGES 18,819–18,833, AUGUST 1, 2000

Global core plasma model

D. L. Gallagher and P. D. Craven
Space Science Department, NASA Marshall Space Flight Center, Huntsville, Alabama

R. H. Comfort
Center for Space Plasma and Aeronomic Research, University of Alabama in Huntsville

Abstract. The global core plasma model (GCPM) provides empirically derived core plasma density as a function of geomagnetic and solar conditions throughout the inner magnetosphere. It is continuous in value and gradient and is composed of separate models for the ionosphere, plasmasphere, plasmapause, trough, and polar cap. The relative composition of plasmaspheric H^+, He^+, and O^+ is included in the GCPM. A blunt plasmaspheric bulge and rotation of the bulge with changing geomagnetic conditions is included. The GCPM is an amalgam of density models intended to serve as a framework for continued improvement as new measurements become available and are used to characterize core plasma density, composition, and temperature.

1. Introduction

By mass, the magnetosphere is dominated by plasma with energies below 100 eV. Beginning with the earliest ground-based whistler [*Storey*, 1953; *Pope*, 1961; *Smith*, 1961] and spacecraft [*Gringauz et al.*, 1960a, b] observations, these core plasmas have been studied for many years. Plasma wave frequencies, particle heating, and instability growth rates can be strongly influenced by the presence and concentrations of core plasmas. Spacecraft charging and the resulting risk of electric discharge and damage to spacecraft electronics can also be mitigated by core plasma.

During these many years of study, quantitative analytical models, based on observations, have been developed for various magnetospheric regions. The work by *Persoon et al.* [1983] is now often used as a reference for polar cap densities. In the plasmasphere and trough the recent work by *Carpenter and Anderson* [1992] can be used. Core plasma densities in the auroral zone might be obtained from the observational paper of *Rycroft and Thomas* [1970], although we are not aware of a statistically derived model for auroral zone core plasma densities. At lower altitudes the models incorporated into the international reference ionosphere (IRI) [*Bilitza et al.*, 1993] are commonly used to represent ionospheric densities at low to intermediate latitudes. Although there has been recent interest in characterizing ionospheric densities at high latitudes, we are not aware of any new high-latitude extensions to IRI or other new empirical models for this region. The work by *Rycroft and Jones* [1985, 1987] provides a description of the ionosphere and plasmasphere by joining the IRI with a diffusive equilibrium model for the plasmasphere.

These models have been developed for the purpose of summarizing observational knowledge about various magnetospheric regions. The values of typical densities and how they vary with location and conditions, such as geophysical and solar activity, have wide-ranging applications. The theoretical modeling of core plasma must relate to observations for guidance and validation. Our understanding of wave-particle interactions and wave propagation must often rely on observationally based typical conditions in regions of interest. Empirical models of magnetospheric conditions also serve as a vital resource in the engineering design and operation of manmade spacecraft systems.

This article acknowledges these applications for magnetospheric core plasma densities by taking the next logical step in the development of practical, empirical products for the space science research and engineering communities through the formation of a global model for core plasma or the GCPM. The GCPM is an integration of region-specific models for core plasma density that have been developed over the years. The objective is to develop an integrated analytical representation that is continuous in value and derivative. The GCPM is intended to take advantage of existing models, including the IRI at low altitudes, and be able to accommodate future advances in empirical modeling of magnetospheric systems. On the basis of the work by *Craven et al.* [1997], this initial GCPM also includes estimates for the relative concentrations of H^+, He^+, and O^+ ions in the plasmasphere. Improvement in the description of ion concentrations and the inclusion of ion temperatures into the GCPM can be accommodated in future versions of the GCPM. Improvements in regional density descriptions will also be needed. One such region is the altitude range between the F_2 peak and ~6000 km. Plasma density measurements are available in this altitude range, but none have yet been used to statistically characterize typical densities in the region. Satellites such as the Defense Meteorological Satellite Program (DMSP) series, Alouette 1, Alouette 2, International Satellite for Ionospheric Studies (ISIS) 1, and ISIS 2 have measured plasma densities in this altitude range and are possible sources for future improvements in the GCPM.

Existing regional models for thermal plasma density do not generally support their use in a continuous, smooth global model. For example, *Carpenter and Anderson* [1992] derive an analytical expression for trough plasma densities, which consists of the concatenation of two linear increases in density with increasing magnetic local time (MLT) from 0 to 15 hours. In another example, neither the plasmaspheric density model of *Gallagher et al.* [1988] nor that of *Carpenter and Anderson* [1992] properly describe the transition of densities from high altitude into the ionosphere. Where possible, the present model builds on existing models. Where not possible, we use satellite measurements and related physical models to sufficiently

Paper number 1999JA000241.
0148-0227/00/1999JA000241$09.00

quantify thermal plasma distributions, so that a complete global picture emerges. Furthermore, with this picture we develop a single, global framework in which existing and future empirical, regional models can be placed.

Although the GCPM depends on the geophysical parameter K_p and the solar luminosity, as given by $F_{10.7}$, it does not include features in magnetospheric density, which result from time-dependent changes. Researchers intending to reproduce the details of observed density fluctuations will find it necessary to make use of time-dependent simulations of the magnetosphere not the GCPM. Empirical characterization of thermal plasma also remains incomplete. The GCPM depends on physical modeling to bridge the gap in high topside ionosphere/plasmasphere measurements. Polar cap density measurements have yet to be quantified in terms of latitude, day-night ionospheric illumination, or geophysical conditions. However, we believe that a "critical mass" of measurements and regional models have been reached for their assimilation into a single global model. The GCPM is a global model that provides reasonable estimates of thermal plasma density throughout the inner magnetosphere and over a range of geophysical conditions. With the GCPM it is hoped that the empirical description of terrestrial thermal plasma will attain a level of structure long enjoyed for the magnetic field and for the ionosphere.

In that context, the authors are engaged in the implementation of the GCPM in FORTRAN computer code. The code will be made widely available upon publication of this work.

2. Overview of the Global Core Plasma Model

The GCPM is intended to provide typical total electron densities and relative concentrations of the major ions for various solar and geophysical conditions. It is also intended to support improvements when new regional models become available in the future. The current GCPM includes the ionosphere, plasmasphere, magnetospheric trough, and polar cap. The IRI is used to represent the ionosphere. Ion densities along auroral field lines are dependent on densities found in the IRI and on the extension of ionospheric densities to magnetospheric altitudes along magnetic field lines. Each region is represented by analytical functions chosen for simplicity or for the capability of associating fit coefficients to physical features of the region. Densities are smoothly varying and available throughout the volume of the inner magnetosphere. Neither the magnetopause nor the plasma sheet are explicitly included in the GCPM; at this time, however, nightside trough densities almost certainly include a near-Earth plasma sheet contribution. There is no explicit outer boundary for the GCPM, but practical use of the current GCPM is limited to the inner magnetospheric region, extending from 90 km out into the plasmaspheric trough. Dayside use of the GCPM may be reasonable into the outer magnetosphere. Nightside use is limited to magnetic field lines, which approximate a dipolar configuration.

A detailed description of the GCPM elements and their derivation are provided in the sections below. Rather than "wading" through that detail first, we present here the features and limitations of the GCPM. Densities are derived as a function of K_p, $F_{10.7}$, the annual mean sunspot number, season, and position. The global K_p index is used to define the location of the plasmapause and bulge and the magnetospheric trough profile. The solar ultraviolet luminosity (through $F_{10.7}$), sunspot number, and date/time are used as input parameters to the IRI, which includes a seasonal dependence. Variations in IRI polar cap densities are currently allowed to raise and lower density along those high-latitude field lines, even though IRI is not well defined at high latitudes. There is also a slight seasonal dependence separately included in the plasmaspheric model [*Carpenter and Anderson*, 1992].

A sampling of the GCPM is presented graphically in Plate 1. From top to bottom, the three rows represent planar slices through the model in the dawn-dusk, noon-midnight, and equatorial planes, respectively. From left to right, the three columns represent states of inner magnetospheric density distribution corresponding to K_p equal to 1, 3, and 5, respectively. Density is color coded, as indicated by the color bar on the right edge. Dashed lines at radial distances of 2, 4, 6, and 8 R_E are shown in the equatorial plane slice, along the bottom row.

Many of the GCPM features can be seen in Plate 1. The first to note in the bottom row is the presence of a blunt plasmaspheric bulge that rotates sunward and decreases in size with increasing geomagnetic activity. The blunt profile differs from the classic teardrop predicted by theory [e.g., *Nishida*, 1966] and that derived empirically for steady state geomagnetic conditions [*Gallagher et al.*, 1995]. This bulge profile corresponds to a statistically derived distribution of plasmapause locations that will be more typical of the distribution of core plasma. The models of *Nishida* [1966] and *Gallagher et al.* [1995] describe theoretical and empirical bulge profiles, respectively, that correspond to the asymptotic conditions of extended steady state convection conditions. The more blunt plasmaspheric bulge profile presented here is believed to better represent the typical distribution of plasma in this region. Also evident in the equatorial images is the diurnal pattern of magnetospheric trough densities. Trough densities vary as $L^{-4.5}$ across L shell (L), increase linearly with MLT starting predawn, and decrease linearly with MLT starting just before the bulge centroid [*Gallagher et al.*, 1998]. Plate 1 (top and middle) shows meridianal slices through the model in the dawn-dusk and noon-midnight planes, respectively. These plots reveal the changing shape of plasma distribution with K_p in the plasmasphere, trough, and polar cap. The dayside polar cap broadens equatorward somewhat with increasing K_p. A shrinking cross section with increasing K_p dominates changes that can be seen in the plasmasphere. A more detailed inspection than that provided in Plate 1 would show that the plasmapause L shell first increases and then decreases near dusk, with increasing K_p, owing to the competition between a sunward rotation of the bulge and a shrinking plasmasphere. Although somewhat difficult to see in this presentation, the noon-midnight slices through the GCPM also show dayside ionospheric and polar cap densities to be enhanced relative to nightside values.

A more quantitative display of GCPM densities is shown in Figure 1. Line plots of density versus geocentric radial distance are shown along the solar magnetic x axis, with the dayside to the left. The outer to inner traces represent successively higher levels of geomagnetic activity for K_p = 1, 3, and 5. Figure 1 is produced for summer conditions and shows somewhat higher densities in the dayside ionosphere. The dayside trough is higher in density than the nightside trough, which also experiences reductions in density owing to the sunward rotation of the plasmaspheric bulge. As mentioned before, trough densities begin to decrease with increasing MLT just westward of the bulge. As the bulge rotates sunward (westward) with increasing activity, the onset of falling trough densities moves to earlier local times, thereby leading to lower trough densities at premidnight local times.

3. The Glue Between Models

There is no single analytical expression that can be used throughout the magnetosphere to represent total electron density, or at least

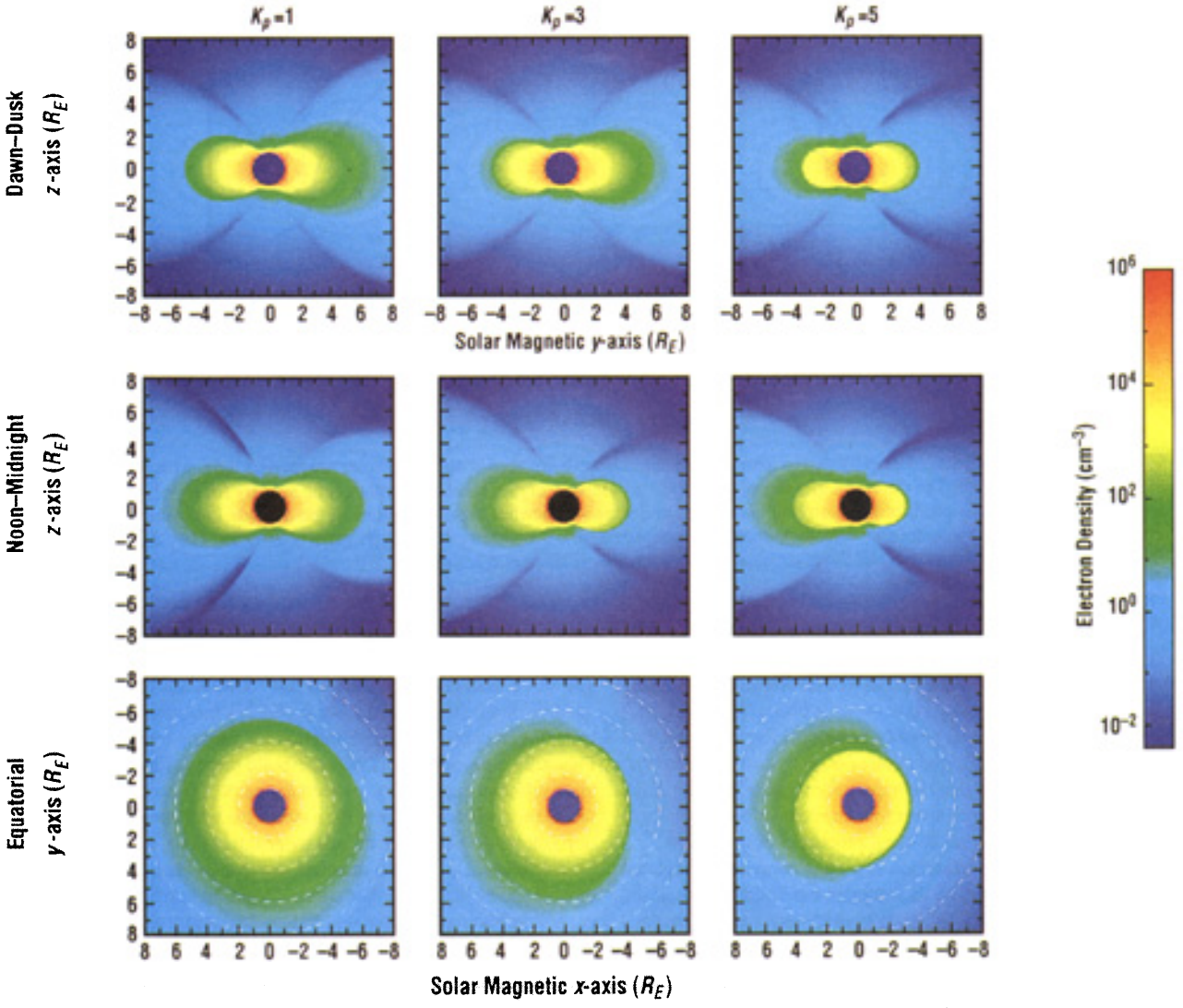

Plate 1. Core plasma densities from the global core plasma model (GCPM) are shown in nine plots, where color is used to indicate density as demonstrated in the color bar at the right. The three columns correspond to low, medium, and high levels of magnetic activity as given by K_p =1, 3, and 5. The top row shows a planar cut in the dawn-dusk meridianal plane. The middle row is the noon-midnight plane. The bottom row is an equatorial cut. The displays are in solar magnetic coordinates.

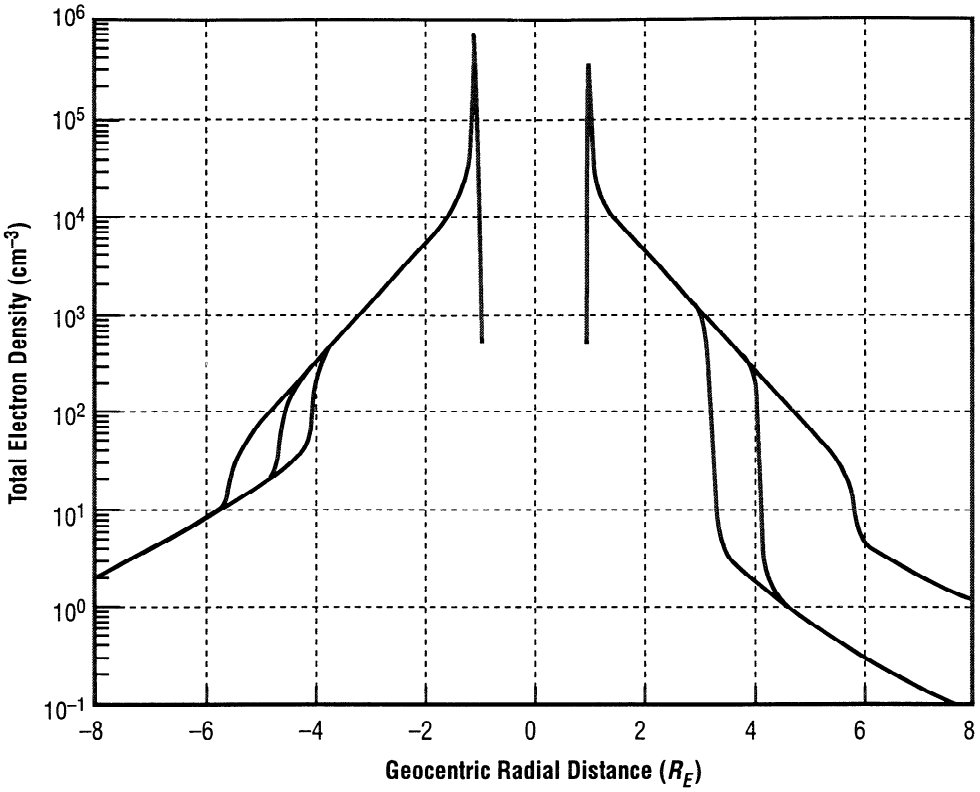

Figure 1. Line plots of density versus geocentric radial distance are shown along the solar magnetic x axis, with the dayside to the left. The outer to inner traces represent successively higher levels of geomagnetic activity for $K_p = 1$, 3, and 5. Figure 1 is produced for summer conditions and shows somewhat higher densities in the dayside ionosphere. The curves demonstrate the smooth joining of ionospheric, plasmaspheric, and trough density models. They also display the usual shrinking of the plasmasphere with increasing magnetic activity.

one that would not be burdened by a large collection of fitted parameters. A series expansion of orthogonal functions would obscure any easy physical insight that might otherwise be obtained from fit coefficients, as compared to other possible functional forms. The method used here is to identify a limited number of analytical functions that are then joined spatially using the hyperbolic tangent function. Each analytical function is chosen either for simplicity or by the ability to relate the function to general physical properties of the region.

The hyperbolic tangent function is used to connect one regional description to another because its argument has unlimited range and the function is asymptotic to ±1. It is used here between regions represented by differing analytical functions to "turn on" one regional empirical model while "turning off" another. To use this function for a variety of spatial transitions, it has been posed in the form

$$y = \frac{\tanh\left(3.4534\dfrac{(x-x_0)}{\Delta x}\right)}{2} + 0.5 \quad , \tag{1}$$

where x_0 is the midpoint for the transition from off to on and Δx is the range over which the transition occurs. The constant (3.4534) in equation (1) is chosen such that the hyperbolic tangent is ≤0.001 or ≥0.999 when $x = x_0 \pm \Delta x$. This will allow us to control the spatial interval of the transition from the empirical model of one region to that of another, in the units of the spatial dimension where the transition is to occur.

Use of equation (1) is illustrated in Figure 2. Two arbitrary power law functions are shown in Figure 2a, labeled 1 and 2. Equation (1) is separately used to "turn off" curve 1 and to "turn on" curve 2, corresponding to potentially different values for x_0 in equation (1). The three dashed curves, labeled 3, 4, and, 5, show the resulting addition of the product of the two power law functions and its corresponding hyperbolic tangent function for varying transition points. Figure 2b shows the pairs of hyperbolic tangent functions for the three different separations between the pairs of functions. The solid line is used with curve 1 and the dashed line with curve 2. Figure 2b (top) shows the pair of hyperbolic tangent functions, where x_0(curve 1) < x_0(curve 2). For this situation, curve 1 in Figure 2a begins to turn off somewhat earlier than curve 2 begins to turn on. The result is curve 3 in Figure 2a. Curve 4 in Figure 2a corresponds to the situation where x_0(curve 1)= x_0(curve 2). Here curve 1 turns off in the same proportion that curve 2 turns on. Curve 5 corresponds to Figure 2b (bottom), where x_0(curve 1) > x_0 (curve 2). Curve 5 in Figure 2a represents the only use of equation (1) where the slope and curvature changes monotonically across the transition between the two original curves. For this reason, the application of equation (1) in curve 5 is the approach used between regional models in the GCPM.

It is through the use of equation (1) that unique functions for each distinct region of the magnetosphere are joined. Functions will be given for the plasmasphere (plasmapause), trough, auroral zone, and polar cap. Equation (1) will be used for model transitions in L shell and altitude. Wherever used, the units for x, x_0, and Δx will be chosen as needed. For example, these units will be in kilometers where a transition in altitude between functions is sought. An alternative is to use one of the Epstein functions introduced by *Booker* [1977] and discussed further by *Rawer* [1984]. These functions are used extensively in the IRI but are not considered for use in the GCPM at this time.

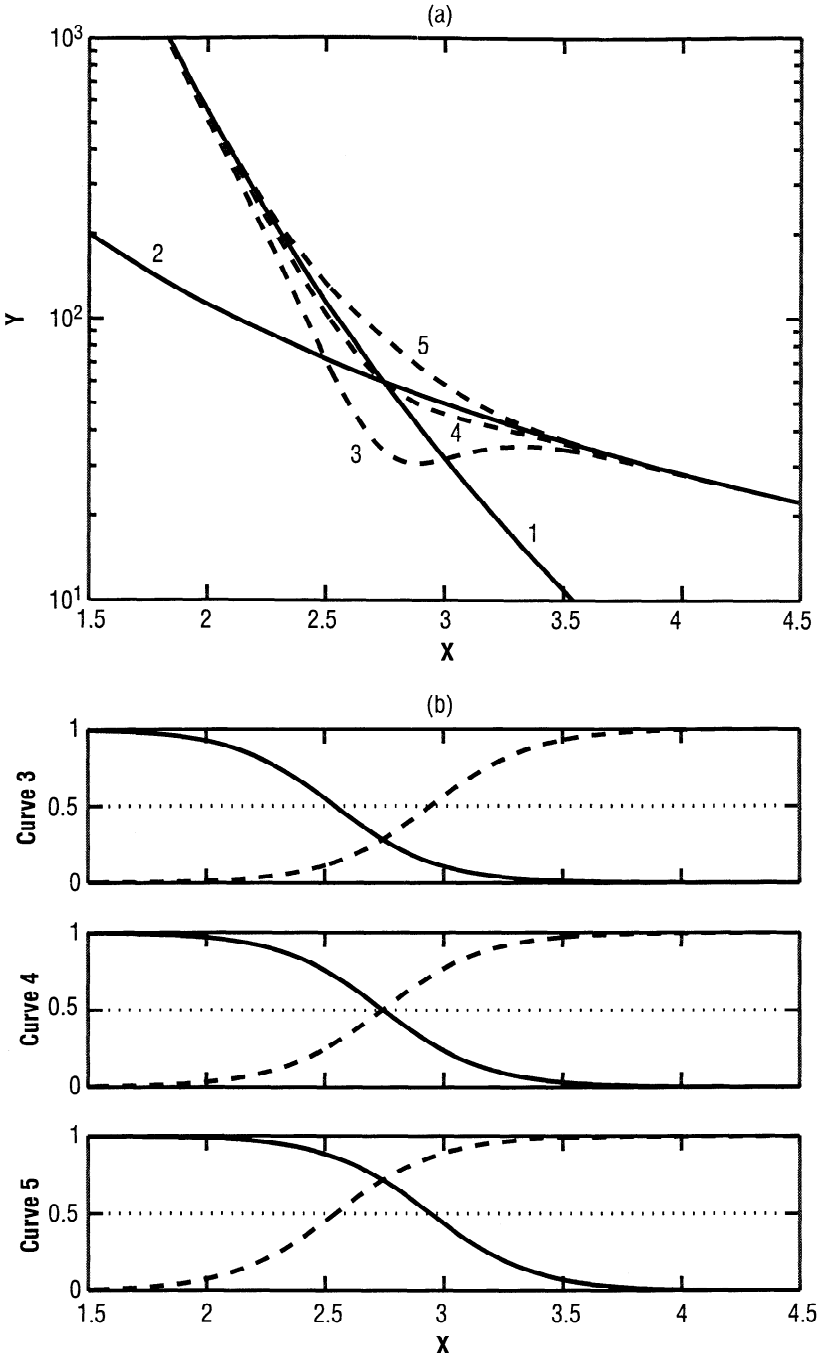

Figure 2. (a) Representative density versus radial distance curves are displayed for the purpose of demonstrating the smooth joining of two intersecting power law density curves (solid lines, numbered 1 and 2). (b) Curves 3, 4, and 5 (dashed lines) in Figure 2a correspond to progressively shifted hyperbolic functions, which are used as coefficients to additively turn off one power law function while turning off the other. The hyperbolic function is used to join independent, regional density models.

4. Plasmasphere and Plasmapause

The plasmasphere and plasmapause electron densities are represented by

$$n_{ps} = 10^{g \cdot h} - 1, \tag{2}$$

where g and h are functions for the inner plasmasphere and for the plasmapause, respectively. Equation (2) is a modification of that used by *Gallagher et al.* [1988], where the term for the ionosphere has been dropped in favor of IRI and where the constant 1 is subtracted from the first term to better support the transition to trough densities. For a saturated plasmasphere the function g can be obtained from *Carpenter and Anderson* [1992],

$$g = (-0.3145L + 3.9043) + \left[0.15\left(\cos\frac{2\pi(t+9)}{365} - 0.075\cos\frac{4\pi(t+9)}{365}\right) + 0.00127\bar{R} - 0.0635\right] e^{-\frac{(L-2)}{1.5}}. \tag{3}$$

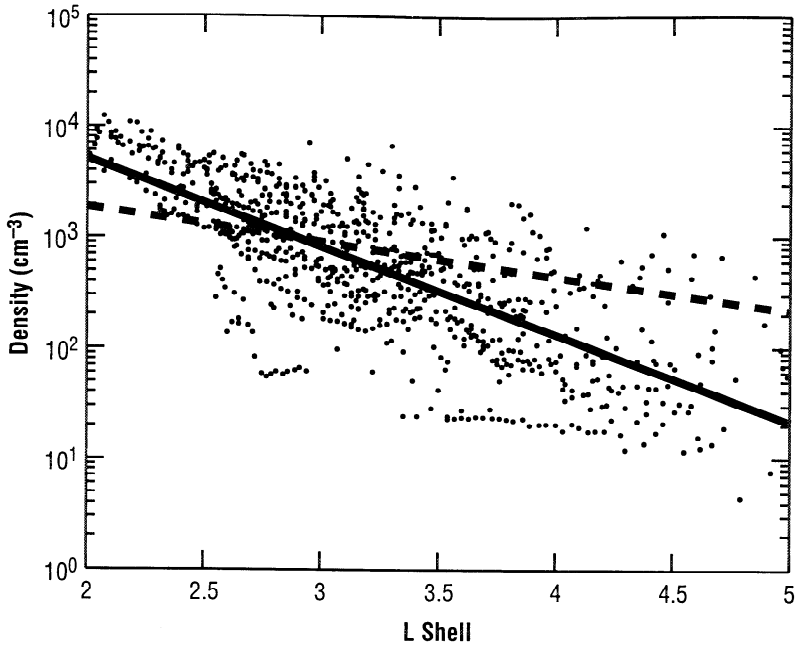

Figure 3. Inner plasmaspheric densities obtained from the Dynamics Explorer 1 Retarding Ion Mass Spectrometer (DE 1/RIMS) instrument are shown in a scatterplot of density versus L shell. Only those densities obtained when the 3-day weighted K_p <1.3, corresponding to extended quiet conditions, are used. All local times and latitudes are included. The solid line is a least squares fit of a straight line to the $\log_{10}$(density) versus L shell. The dashed line is the saturated density function obtained from *Carpenter and Anderson* [1992].

The plasmaspheric densities given by equation (3) depend on L, the day of the year t, and the 13-month-average sunspot number $\overline{R}$. Equation (3) does not depend on MLT; therefore it represents an azimuthally symmetric inner plasmasphere. The diurnal variations commonly observed in the ionosphere are not readily evident in the plasmasphere. The first term in equation (3) represents the large-scale dependence of density on L shell inside the plasmasphere. The second term contains the small seasonal and sunspot number dependencies of plasmaspheric density derived by *Carpenter and Anderson* [1992]. It is not appropriate, however, for the GCPM to represent saturated plasmaspheric densities, as it is our intent that the GCPM represent typical densities. The more typical situation is that outer plasmaspheric L shells will be less well filled owing to continuous random erosion resulting from fluctuations in the convective electric field. The more interior the plasmaspheric L shell, the less often it will be affected by convective erosion. The expectation is that densities inside the plasmapause will often be more sharply decreasing with L than that represented in equation (3). *Gallagher et al.* [1988] obtain a logarithmic plasmaspheric density slope ranging from −0.87 to −0.75, corresponding to noon and midnight MLTs, respectively. More complete first-moment analysis data of Dynamics Explorer 1 Retarding Ion Mass Spectrometer (DE 1/RIMS) are now available than was used by *Gallagher et al.* [1988]. A sample of that data is shown in Figure 3, where density is plotted versus L shell. These total densities are obtained from measurements made during quiet geomagnetic conditions for all local times and latitudes inside the plasmasphere. Quiet conditions were chosen to ensure that only those measurements inside the plasmasphere are included; however, nothing has been done to specifically limit the data set to saturated flux tube conditions. The solid line represents a linear least squares fit to the logarithm of density, which is given by

$$\log_{10}(n_e) = -0.79L + 5.3 \quad . \tag{4}$$

The dashed line is obtained from the *Carpenter and Anderson* [1992] expression given in equation (3) and is based on measurements between 0 and 15 hours MLT. What is clear from this comparison is that more needs to be done to characterize both typical and saturated densities in the plasmasphere. At low L shells, *Carpenter and Anderson* [1992] find saturated plasmaspheric densities clearly below that measured by the DE 1/RIMS instrument. However, the *Carpenter and Anderson* [1992] densities were obtained using the International Sun Earth Explorer 1 Plasma Wave Instrument (ISEE 1/PWI) and under different solar cycle conditions than those by DE 1/RIMS. The DE 1/RIMS-derived density values, used in Figure 3, do not show significant dependence on MLT. Therefore the differences between local time sampling in our data set and that of *Carpenter and Anderson* [1992] do not appear to be the source of the differences in the derived inner plasmaspheric density gradient. An independent study of plasmaspheric densities using DE 1/RIMS, DE 1/PWI, and ISEE 1/PWI is being conducted and will be reported. In the interim, the interior plasmaspheric density profile given by equation (4) will replace that for saturated densities in equation (3) in the current GCPM, as shown in equation (5). In addition, the seasonal and sunspot number dependence for inner plasmaspheric density obtained by *Carpenter and Anderson* [1992] is retained in equation (5):

$$g = (-0.79L + 5.3) + \left[0.15 \left(\cos\frac{2\pi(t+9)}{365} - 0.075\cos\frac{4\pi(t+9)}{365} \right) + 0.0127\overline{R} - 0.0635 \right] e^{\frac{(L-2)}{15}} \quad . \tag{5}$$

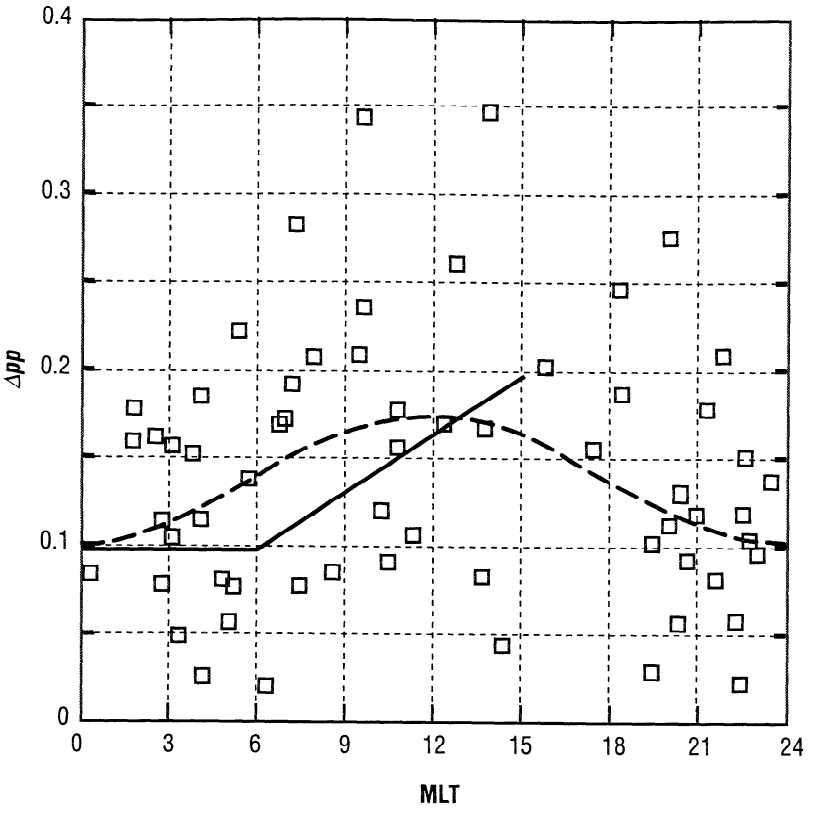

Figure 4. Plasmapause slope values from *Carpenter and Anderson* [1992] are plotted against MLT as open squares. The solid line is the model fit from *Carpenter and Anderson* [1992] for the MLT range from 0 to 15 hours. The dashed line results from fitting a sinusoidal curve to the data.

The importance of these additional dependencies remains to be determined by a more complete study. The function h is from *Gallagher et al.* [1988],

$$h=\left(1+\left(\frac{L}{a_8}\right)^{2\cdot(a_9-1)}\right)^{\left(\frac{-a_9}{(a_9-1)}\right)} . \quad (6)$$

The fitted parameters in equation (6) are defined so that the plasmapause location and slope reproduce that derived by *Carpenter and Anderson* [1992], except for the presence of a slight bulge. The term a_8 is the location of the midpoint of the plasmapause density falloff. The term a_9 controls the plasmapause gradient. Both terms are a function of the maximum K_p in the preceding 24 hours, referred to as $K_{p_{\max}}$. The plasmapause gradient, as presented by *Carpenter and Anderson* [1992], varies with MLT, and hence the term a_9 also varies with MLT. The plasmapause gradient or scale width (Δpp) is defined by *Carpenter and Anderson* [1992] to be piecewise continuous in two linear segments:

$$\Delta pp = 0.1 \quad 00 \le t \le 06 \text{ MLT}$$

$$\Delta pp = 0.1 + 0.011\,(t-6) \quad 06 \le t \le 15 \text{ MLT} .$$

The plasmapause scale width, as defined by *Carpenter and Anderson* [1992], is

$$\Delta pp = \frac{\Delta L_{pp}}{\Delta \log(n_e)} ,$$

where ΔL_{pp} is the L shell width of the plasmapause and corresponds to the fractional density drop across the plasmapause.

For our application the term a_9 must be both continuous and periodic; therefore we have revisited the derivation of Δpp by reproducing Figure 9a from *Carpenter and Anderson* [1992] in our Figure 4. To Figure 4 we have added the fit provided by *Carpenter and Anderson* [1992] as the solid line. The derived values for Δpp appear to peak near noon and minimize near midnight, even though the variation is small relative to the scatter. To produce a periodic expression for the terms in equation (6), a sinusoidal function is least squares fit to the Δpp values in Figure 4. The fitted sinusoid peaks just after 12 hours MLT, but owing to the limited statistics and scatter in Δpp the peak is placed at noon, and the fit is plotted as a dashed line in Figure 4. The dashed line for Δpp is given by

$$\Delta pp = 0.036\sin\left(\frac{2\pi(\text{MLT}-6)}{24}\right)+0.14 . \quad (7)$$

Equations (5) and (7), when combined with a location for the plasmapause, define the density profile for the plasmasphere and plasmapause. However, they do not directly define the values for a_8 and a_9 to be used in equation (6) in the GCPM. As an initial step to obtain these quantities, equation (8) is fit to the density profile defined by equations (5) and (7), assuming the plasmapause L shell (L_{ppi}) as a function of $K_{p_{\max}}$ derived by *Carpenter and Anderson* [1992]:

$$L_{ppi} = 5.6 - 0.46K_{p_{\max}} .$$

Therefore, before including a bulge in the plasmapause azimuthal profile, the fitted values for a_8 and a_9 are found to be

$$a_8 = b_1 K_p + b_2$$
$$a_9 = b_3 K_p + b_4 \quad , \tag{8}$$

where

$$b_1 = 0.0027\cos\left(\frac{MLT}{12}\pi\right) - 0.448$$

$$b_2 = 0.0373\cos\left(\frac{MLT}{12}\pi\right) + 5.747$$

$$b_3 = 0.8352\cos\left(\frac{MLT}{12}\pi\right) - 3.809$$

$$b_4 = -8.415\cos\left(\frac{MLT}{12}\pi\right) + 41.53 \quad .$$

Although already stated, it is worthwhile to call attention to the basis for equation (8) again. Equation (8) defines the parameters that are used in equation (6) to define the location and slope of the plasmapause. These parameters have been derived so that equation (6) reproduces the plasmapause properties derived by *Carpenter and Anderson* [1992]. Not yet included is the extension of cold plasma in the bulge region.

To more fully address the azimuthal distribution of near-Earth dense plasma, it is necessary to be clear about our objective. References to plasmaspheric plasma most often bring with it an implicit assumption about the convective motion of that plasma; that is, that magnetic flux tubes containing the plasmasphere corotate with the Earth. Our interest here, however, is to identify typical core plasma densities, regardless of whether that plasma is on closed, open, or stagnant convective paths. As reviewed below, an extension of dense plasma often exists near evening local times and has often been referred to as the plasmaspheric bulge. Whether this plasma convects on Earth-encircling trajectories or is a nearly stagnant accumulation of plasma outside the plasmasphere, its frequent presence identifies it as important to our study. Therefore, although we will use the language of those we reference to discuss their observations of core plasma in the bulge region, we do not address the convective motion of core plasma.

With that in mind, our first step is to review studies that have empirically characterized the azimuthal or bulge density profile. Table 1 summarizes the results. Some studies have found the azimuthal distribution of plasma to be symmetric. Each of those studies has an entry in the symmetric data column in Table 1. The entries describe any limitations relevant to their determination of a symmetric plasma distribution. For example, the *Carpenter and Smith* [1964] result is limited to the analysis of densities at L=3. The *Gringauz and Bezrukikh* [1976] study is limited to conditions of high K_p. It is evident from Table 1 that azimuthal density profiles are symmetric for the inner L shells and low altitudes.

Also clear is that there often exists an extension of dense plasma to higher altitudes at evening local times. A few studies identify an evening bulge distribution that is rounded in local time, such as that

Table 1. Local Time Profile of the Plasmapause

Source	Symmetric	Rounded	Teardrop	Rotation
Carpenter and Smith [1964]	L=3			
Taylor et al. [1965]	L<5			
Carpenter [1966]	low K_p		moderate K_p	
Binsack [1967]	$K_p \leq 1$		hint	
Carpenter [1970]		yes		yes*
Chappell et al. [1970]			consistent	
Taylor et al. [1970]			consistent	
Chappell et al. [1971]		18 hours MLT		
Freeman [1973]†			yes	
Gringauz and Bezrukikh [1976]	high K_p			
Brace and Theis [1974]	3000 km			
Maynard and Grebowsky [1977]		postdusk		
Park et al. [1978]	3<L<4.5			
Knott et al. [1979]	at 100 cm^{-3}			
Decreau et al. [1982]			near 18 hours MLT	
Higel and Lei [1984]			consistent	yes
Gallagher et al. [1988]	L<3	L>3		
Comfort et al. [1988]	L<4.5	L>4.5	L>4.5	
Horwitz et al. [1990]	high K_p			
Carpenter and Anderson [1992]	0–15 hours MLT			
Moldwin et al. [1994]	highly structured	highly structured	highly structured	yes
Gallagher et al. [1995]			yes	

*Activity is high in the afternoon, steady at 18 hours MLT, and quiet at 19–20 hours MLT.
†See *Rycroft* [1975].

by *Carpenter* [1970]. *Chappell et al.* [1971] found a rounded bulge centered at18 hours MLT. *Maynard and Grebowsky* [1977] find a rounded bulge centered at postdusk local times. *Comfort et al.* [1988] found the distribution of plasma to be symmetric inside $L=4.5$ and extended or bulged outside this L shell. More sharply bulged or teardrop distributions have also been identified. *Carpenter* [1966] reports a teardrop profile for moderate K_p conditions. *Chappell et al.* [1970], *Taylor et al.* [1970], and *Higel and Lei* [1984] report their observations to be consistent with a teardrop profile, while *Binsack* [1967] only shows evidence that hints at that profile. When measurements have been sensitive to local time movement of bulge plasmas with varying magnetic activity, the bulge has been found to move toward earlier MLT with increasing activity, as documented in the rotation data column in Table 1. *Gallagher et al.* [1995] derived a strongly teardrop-shaped plasmasphere but only for prolonged, steady geomagnetic conditions. Our interest here is to characterize typical densities of core plasma, which can be expected to have distributions somewhere between symmetric and teardrop.

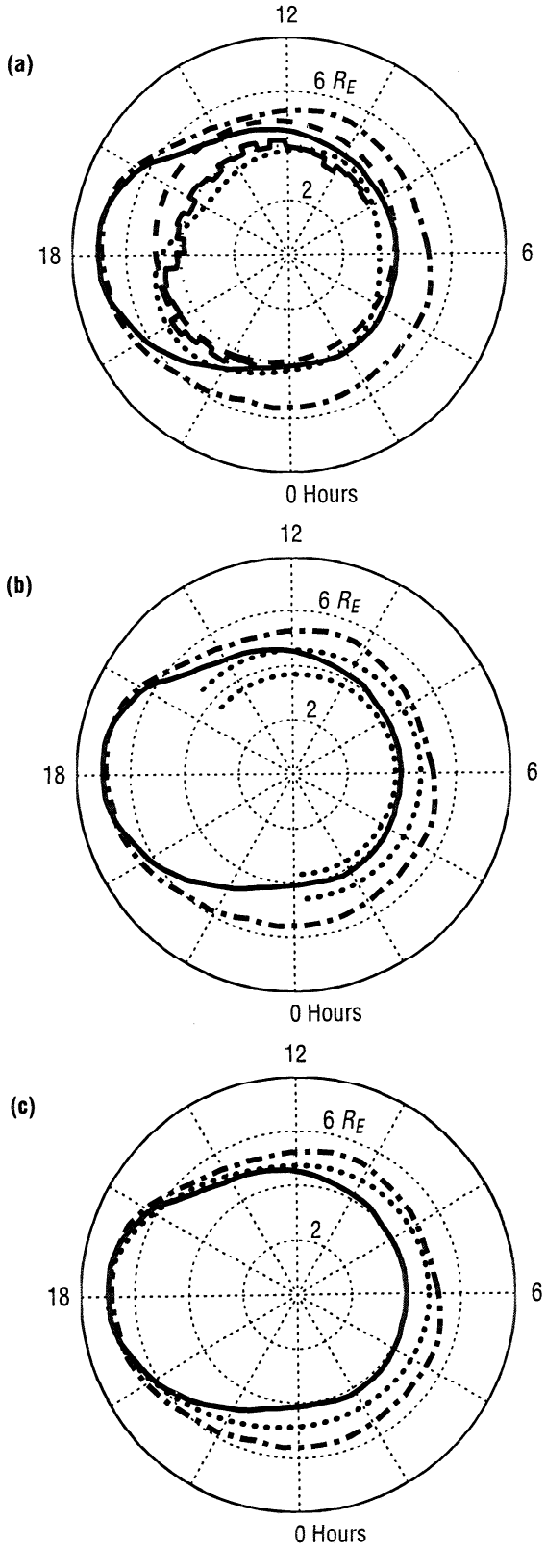

Figure 5a shows the statistical azimuthal plasmapause location presented by *Carpenter* [1966] (dotted line), *Taylor et al.* [1970] (dot-dashed line), *Chappell et al.* [1971] (outer solid line), *Maynard and Grebowsky* [1977] (inner solid line), and *Gallagher et al.* [1988] (dashed line). Three of the studies reveal remarkably similar plasmapause profiles [*Carpenter*, 1966; *Maynard and Grebowsky*, 1977; *Gallagher et al.*, 1988]. Each of these three studies tended toward the identification of the innermost plasmapause boundaries. *Carpenter* [1966] specifically states that the innermost knee of a gradient in plasmaspheric density was selected on the basis of ground whistler observations. *Maynard and Grebowsky* [1977] relied on saturation of the direct current double-probe instrument on Explorer 45, which occurs near a density of 65 cm^{-3}. The *Gallagher et al.* [1988] study selectively studied plasmaspheric density profiles that were smooth, with only a single, sharp plasmapause. Such simple density profiles appear to most often identify the region *Carpenter et al.* [1993] describe as the main plasmasphere, a region that does not include the bulge. Bulge plasmas appear to result from time-varying convection, which typically leads to a more structured distribution of plasma with L shell in the dusk region. For this reason, the studies of *Carpenter* [1966], *Maynard and Grebowsky* [1977], and *Gallagher et al.* [1988] tend to exclude significant portions of the distribution of thermal plasma in the outer dusk region.

Studies by *Taylor et al.* [1970] and *Chappell et al.* [1971] identified their boundary locations by finding sharp density gradients. *Taylor et al.* [1970] additionally required that a steep density dropoff be followed by at least three consecutive low-density samples. They report that densities in the outer dusk plasmasphere become highly structured during times of changing activity. The additional requirement that low densities persist following a sharp density drop, with increasing L shell, appears to have the effect of including outer plasmaspheric structures inside their identification of the plasmapause

Figure 5. (a) The statistical azimuthal plasmapause location presented by *Carpenter* [1966] (dotted line), *Taylor et al.* [1970] (dot-dashed line), *Chappell et al.* [1971] (outer solid line), *Maynard and Grebowsky* [1977] (inner solid line), and *Gallagher et al.* [1988] (dashed line) is shown. (b) The plasmapause profile shown with the dot-dashed curve is from *Taylor et al.* [1970], and the solid curve is from *Chappell et al.* [1971]. To these curves, two dotted partial circles have been added. These curves correspond to the inner edge of the plasmapause boundary identified by *Carpenter and Anderson* [1992] for $K_p=2$ and 4 (outer and inner dotted curve, respectively). (c) This plot repeats the same azimuthal density profile as Figure 5(b), but this time two new dotted curves have been added. These curves are based on the *Carpenter and Anderson* [1992] variation of plasmapause L shell, with a bulge profile based on fits to the *Taylor et al.* [1970] and *Chappell et al.* [1971] azimuthal density profiles at different levels of magnetic activity. The outer and inner dotted curves correspond to $K_p=0.9$ and 3.5, respectively, in equation (9).

boundary. The *Chappell et al.* [1971] study was sensitive to densities down to 0.1 cm^{-3} and apparently also includes closely spaced density structures within identified plasmaspheric boundaries. The implication is that these two studies consistently include dense thermal plasma in the bulge region, outside of the main plasmasphere [*Carpenter et al.*, 1993].

An additional perspective might be gained by comparing these two azimuthal density profiles with that given by *Carpenter and Anderson* [1992], as done in Figure 5b. Again, the dot-dashed curve is from *Taylor et al.* [1970], and the solid curve is from *Chappell et al.* [1971]. To these curves, two dotted partial circles have been added. These curves correspond to the inner edge of the plasmapause boundary identified by *Carpenter and Anderson* [1992] for K_p = 2 and 4 (outer and inner dotted curve, respectively). There is sufficient correspondence between these curves near dawn to suggest that the deviation of the azimuthal profiles away from a circular shape at other local times is what we need here to include bulge plasmas in our description of typical "plasmaspheric" densities. The *Chappell et al.* [1971] and *Taylor et al.* [1970] plasmapause profiles are reported to include a similar range of geomagnetic activity. Both also show considerable scatter.

Figure 5c repeats the same azimuthal density profiles, but this time a new dotted curve has been added. This curve is based on the *Carpenter and Anderson* [1992] variation of plasmapause L shell at dawn, with a bulge profile based on a fit to the average of the *Taylor et al.* [1970] and *Chappell et al.* [1971] azimuthal density profiles. The expression used to create this fit is based on the approach presented by *Gallagher et al.* [1995]:

$$L_{pp} = \left(5.6 - 0.46K_p\right)\left[1 + f(x)\right]$$
$$f(x) = e^{\left(-1.5x^2\right)+0.08x-0.7}, \quad (9)$$

where x is the azimuthal angle relative to the bulge centroid in radians. The form of equation (9) is chosen so as to isolate the main plasmasphere (first term) from the bulge profile (second term). For Figure 5c the bulge centroid is located at 18 hours MLT. For equation (9) to be incorporated into equation (6) through the parameter a_8 in equation (8), it is necessary to restate a_8 as

$$a_8 = \left(b_1K_p + b_2\right)\left[1 + e^{\left(-1.5x^2+0.08x-0.7\right)}\right]. \quad (10)$$

Note that equation (10) retains the dawn plasmapause position as a function of geophysical activity derived by *Carpenter and Anderson* [1992] as well as the variation of the plasmapause gradient given in equation (7). This final expression for a_8 now also contains the extension of thermal plasma typically observed in the evening sector. The form of equation (10) also leads to a reduction in the size of the plasmasphere with increasing activity derived by *Carpenter and Anderson* [1992]. The same inward motion of the plasmapause with increasing K_p derived for dawn is applied to all local times, including the bulge region.

As mentioned earlier, the rotation of bulge plasmas sunward with increasing geomagnetic activity has often been observed (Table 1) and should be included in our description of typical conditions. An expression for the MLT location of the bulge center is derived by *Gallagher et al.* [1995] to be

$$\Phi_B(\text{hours}) = \frac{47}{K_p + 3.9} + 11.3 . \quad (11)$$

This result is based on the statistical observations of *Higel and Lei* [1984] and *Moldwin et al.* [1994]. Equations (10) and (11) are used together to define the plasmapause and bulge location in the GCPM. The equations are combined by using equation (11) to define the MLT corresponding to x=0 in equation (10).

The relative concentration of He^+ to H^+ ions in the plasmasphere can be obtained from *Craven et al.* [1997]. These authors empirically derive the following expression for the ratio:

$$\log_{10}\left(\frac{n_{He^+}}{n_{H^+}}\right) = -1.541 - 0.176r + 8.557\times10^{-3}P - 1.458\times10^{-5}P^2 , \quad (12)$$

where r is radial distance in R_E and P is a proxy measure of solar activity derived by *Richards et al.* [1994]. It is defined as

$$P = \frac{\left(F_{10.7} + F_{10.7A}\right)}{2} ,$$

where $F_{10.7}$ is the 81-day average of the daily 10.7-cm solar flux ($F_{10.7}$). Relative O^+ concentrations are derived for early DE 1 RIMS measurements by *Comfort et al.* [1988]. In this study, the ratio of O^+ to H^+ density is found to vary from ~1% in the morning to as high as 10% in the local evening. Concentrations are also found to minimize near L=2 and increase toward the outer plasmasphere. The RIMS measurements used in this study were obtained during October and November 1981 shortly after the launch of DE 1. This was a period of high solar activity and moderate, variable magnetic activity. The current availability of the entire DE 1/RIMS data set suggests that this analysis can be extended to provide a more complete description of O^+ concentrations throughout the plasmasphere and for varying geomagnetic conditions. That analysis will be left for later study. Here we will adopt a constant 1% relative concentration of O^+ to H^+ in the plasmasphere. Also, left for later development is the smooth transition between IRI ion concentrations in the ionosphere and those found in the plasmasphere. Using equation (12) and our assumption for O^+ plasmaspheric concentrations, the density for each of these three ions can be described by

$$n_{He^+} = R_{He^+} n_{H^+}$$
$$n_{O^+} = R_{O^+} n_{H^+}$$
$$n_{H^+} = \left(1 + R_{He^+} + R_{O^+}\right) n_e ,$$

where each equation gives the corresponding ion density, where R_{He^+} and R_{O^+} are the corresponding ion density ratios with H^+ and where n_e is the total electron density.

5. The Trough

The trough density model suggested for static conditions by *Gallagher et al.* [1995] will be used in the GCPM. In this empirical model, nighttime densities at geosynchronous orbit are assumed to minimize at 0.18 cm^{-3} between 1 and 3.5 hours MLT. Filling starts near 3.5 hours MLT at a rate of 0.56±0.08 $cm^{-3}\,h^{-1}$ until reaching an MLT given by

$$\Phi_{TP} = 0.145K_p^2 - 2.63K_p + 21.86 \text{ hours}. \quad (13)$$

The *Gallagher et al.* [1995] studies report a density decrease at a rate of -0.83 ± 0.15 cm^{-3} h^{-1} following the MLT given in equation (13). The decrease begins just before the bulge centroid. The bulge centroid MLT rotates eastward with decreasing activity. If activity is low enough, the onset of decreasing trough densities may not start early enough in MLT to reach the level previously stated for the postmidnight sector. In a time-dependent analysis like that done by *Gallagher et al.* [1995] this does not present a problem. The appearance of a higher density at midnight translates into higher densities in the following day as trough plasma convects into and across the dayside. In a static model, like the GCPM, it is necessary to ensure that the description of trough density is periodic and continuous through midnight, without a discontinuity. To accommodate the eastward rotation of the bulge with decreasing activity, the rate of trough density decrease may need to be advanced to ensure that a discontinuity at midnight is avoided. Trough density is assumed to return to the nighttime minimum density stated above and the rate of density decrease is increased, if necessary, to accomplish that result.

The variation of trough density with L shell is taken from *Carpenter and Anderson* [1992]. In that paper, trough density is found to vary with $L^{-4.5}$. Therefore densities throughout the trough are determined by first finding the density at geosynchronous orbit, which is defined above in text and equation (12), and then by scaling in L shell.

6. Low-Altitude Transition: Plasmasphere and Trough to IRI

Plasmaspheric and trough densities observed by *Gallagher et al.* [1988] and *Carpenter and Anderson* [1992] extend inward only to ~2 R_E. The IRI can be used up to ~600 km, where IRI densities become constant at unrealistically high values. The solid line in Figure 6 shows the densities returned by IRI along an $L=2$ field line for arbitrarily chosen conditions and local time. The single dot shows the corresponding equatorial density returned by the plasmaspheric model. The dashed curves in Figure 6 show the IRI and plasmaspheric density profiles along the geomagnetic equator. All densities are for 12 hours MLT. These profiles along and across the magnetic field are globally representative of the inherent discontinuity that exists between the IRI and the GCPM plasmaspheric model. Figure 6 demonstrates that a transition must be made between the steep topside ionospheric densities from IRI and our plasmaspheric empirical model.

Interpolating between the topside ionospheric profile of IRI and the plasmaspheric density profile, using the following power law function, accomplishes the necessary transition in altitude:

$$n_e = e^{\frac{d}{d_0}+d_1}, \tag{14}$$

where d is the altitude in kilometers and d_0 and d_1 are constants. The origin of equation (14) is discussed below. Along the magnetic equator, equation (14) is separately used to extend densities upward from the ionosphere and downward from the plasmasphere. The transition from IRI to the extrapolated curve is made at the altitude of the maximum negative density gradient above the F_2 peak. The free parameters, d_0 and d_1, in equation (14) are fit to the slope and density at this point. Equation (14) is separately fit to the equatorial plasmasphere density gradient, so that it is extended inward across L shells. The transition in density at the intersection of the two fitted versions of equation (14) is smoothed by equation (1), as is the transition just above the F_2 peak. It is in this way that continuous values in equatorial density are derived for the ionosphere, through the plasmasphere, and into the trough.

A somewhat similar operation is performed to obtain densities away from the magnetic equator along magnetic field lines. However, equation (14) is only applied once to extend ionospheric density outward along plasmaspheric and trough field lines. The free parameters in equation (14) are again determined at the height of maximum negative density gradient above the F_2 peak, except that a

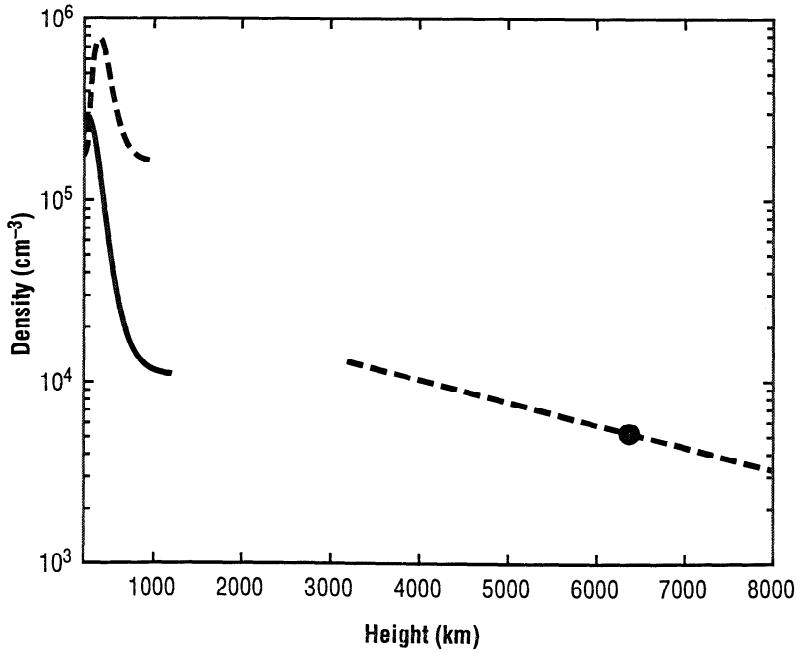

Figure 6. Density versus height are shown along the $L=3$ magnetic field line (solid line and single dot) and along the magnetic equator (dashed lines) from the international reference ionosphere (IRI) and plasmasphere models. The curves demonstrate the limitation of the IRI topside densities above ~600 km and the need to interpolate between the ionospheric and plasmaspheric models.

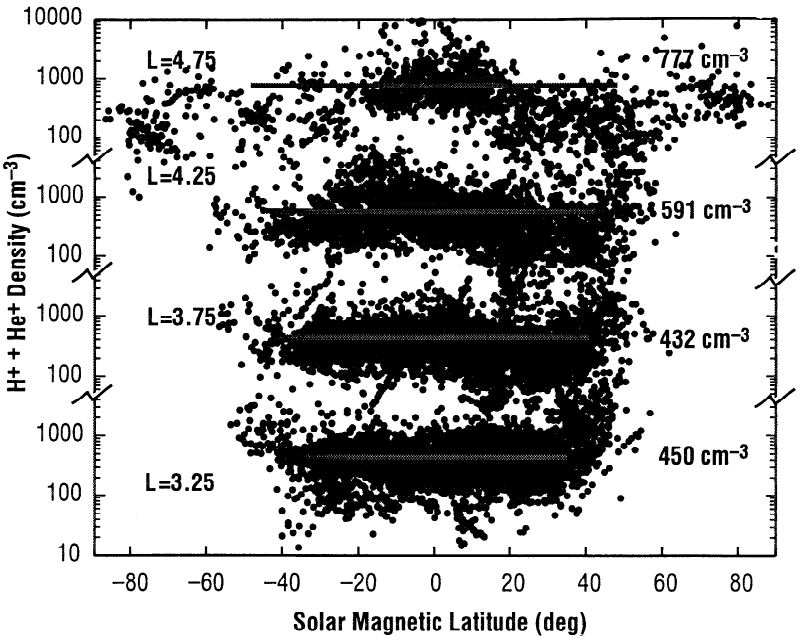

Figure 7. The sum of H^+ and He^+ densities from the DE 1/RIMS instrument are shown in a concatenated, "broken" density scale versus solar magnetic latitude. For all magnetic activity conditions and local times the densities are grouped into four 0.5-wide L shell ranges centered at $L=3.25$, 3.75, 4.25, and 4.75. The solid horizontal lines are the mean densities in each L shell "bin" with these average values shown on the right. The solid lines extend to latitudes corresponding to geocentric distances of 2 R_E in the Northern and Southern Hemispheres. The density along L shells is found to be without significant trend with latitude down to this distance.

constant additive term is included in equation (14). The purpose of this term is to cause the function to become asymptotic at the equatorial density for a given L shell.

Previous studies of core plasma density variation near the equator and along magnetic L shells have seen little variation with latitude [e.g., *Decreau et al.*, 1986]. A notable exception is the work by *Angerami and Carpenter* [1966], who found field-aligned density variations consistent with diffusive equilibrium in the plasmasphere and with $1/R^4$ in the trough. To complete the GCPM along plasmaspheric and trough field lines, it is necessary to quantify the density variation along field lines.

Figure 7 is a composite plot of density versus latitude, inside the plasmasphere, from the RIMS on the DE 1 spacecraft. All available reduced plasmasphere measurements from RIMS in four L shell ranges and for all geomagnetic conditions and local times are shown in this scatterplot. Immediately evident is the remarkable, nearly constant value of density in each of the 0.5-wide L shell ranges, centered at $L=3.25$, 3.75, 4.25, and 4.75. The solid lines show the average density for each L shell range. The line length is chosen to extend down to an altitude of 1 R_E for the middle of each L shell range. That altitude is chosen because it appears that the core plasma density remains nearly constant from the equator down to that altitude, particularly at the lower L shells.

Note in Figure 7, at the highest L shell range presented, that a density increase appears to be present within ~20° latitude of the magnetic equator. Individual pass plots of density versus latitude, derived from the PWI on DE 1, have been separately examined for those times when DE 1 is outside the plasmapause in the trough. These data also show very little systematic variation of density with latitude, although measurements near the magnetic equator and in the trough are limited on DE 1. To the extent that any systematic variation is evident, the DE 1/PWI-derived densities often show a profile that appears similar to that shown with DE 1/RIMS measurements in the $L=4.75$ "bin" plotted in Figure 7. That is, PWI also observes an increase in density near the magnetic equator. Enhanced density at the equator might be associated with flux tube filling; however, that is in contrast with *Olsen et al.* [1987], who reported essentially constant density across the equator in the vicinity of the plasmapause. The relatively small equatorial variation in density found at the highest L shell in Figure 7 is not included in this version of the GCPM. It is assumed that the density in both the plasmasphere and trough regions is nearly constant along L shells down to an altitude of 1 R_E.

At high altitudes the power law in altitude used here to represent density variation along L shells is little different from a power law in radial distance. The equatorial densities, determined above, constrain the field-aligned profile at the top of the field line. The IRI constrains the profile at its base. It is at lower altitudes where the difference between radial distance and altitude power laws become great. Relative to the power law in radial distance, the power law in altitude rises rapidly at low altitudes. The form of equation (14) was chosen because it corresponds to that most often found (P. D. Craven, private communication, 1999) in flux tube modeling with the field line interhemispheric plasma model [*Torr et al.*, 1990; *Richards et al.*, 1991; *Craven et al.*, 1995]. The altitude power law satisfies the need to connect the relatively high densities of the topside ionosphere with the low densities of the plasmasphere and trough. It also yields a relatively flat density profile at high altitudes, which is not measurably different from a constant value near the equator. The result of adopting the presented altitude power law profile for density along field lines in the plasmasphere and trough leads to a similar, favorable comparison to Alouette densities as that performed by *Angerami and Carpenter* [1966, Figures 14 and 15]. A much more complete analysis of the validity of the power law interpolation be-

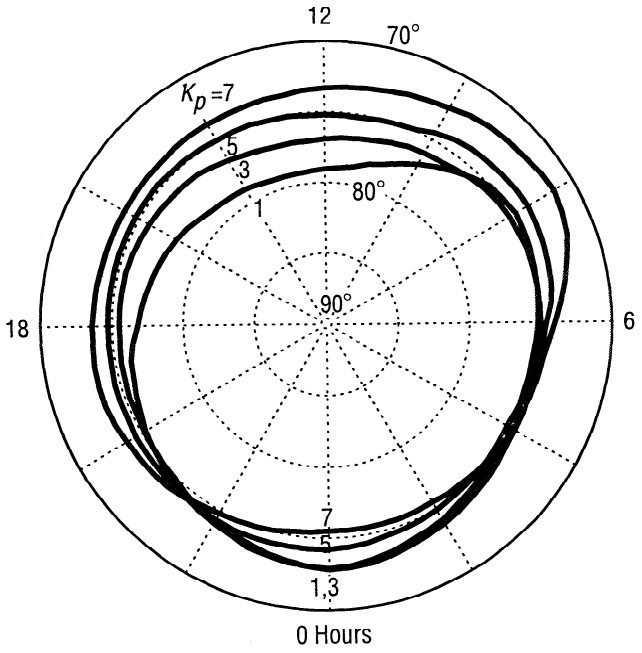

Figure 8. Solid lines mark the poleward edge of the auroral oval obtained from *Comfort* [1972] and *Feldstein and Starkov* [1967, 1968]. Azimuthal angle in the dial plot is solar MLT. Magnetic latitude is shown radially down to 50°, with circles drawn every 10°. The innermost to the outermost line corresponds to K_p=1, 3, 5, and 7.

tween IRI and plasmaspheric densities can be performed with densities measured by the Air Force DMSP satellites. That study has been initiated and results will be reported later (F. Rich, private communication, 1999).

7. Polar Cap

In the polar cap the density variation along field lines is assumed to transition from that described previously to something similar to that by *Persoon et al.* [1983]. The latitude for the poleward edge of the auroral zone is obtained from *Comfort* [1972] and *Feldstein and Starkov* [1967, 1968]. These papers provide a simple, K_p-dependent location for the poleward edge of the auroral oval used here to allow separate treatment of polar cap and lower latitude field line densities. The location of the poleward edge of the auroral oval, based on these references, is shown in Figure 8 for values of K_p=1, 3, 5, and 7. The transition between closed and open magnetic field line density profiles will be accomplished using equation (1), where the transition is centered at the poleward edge of the auroral oval and occurs over an L shell range of ±1. A more complete treatment for defining the auroral zone as a function of the interplanetary magnetic field and geophysical activity is available but will be left for future addition to the GCPM.

The density profile in the polar cap will be obtained from the work of *Persoon et al.* [1983]. Persoon et al. used measurements by the PWI on the DE 1 spacecraft to derive densities as a function of radial distance in the polar cap. Those averaged values are reproduced with asterisks in Figure 9, where in this case, densities are plotted versus

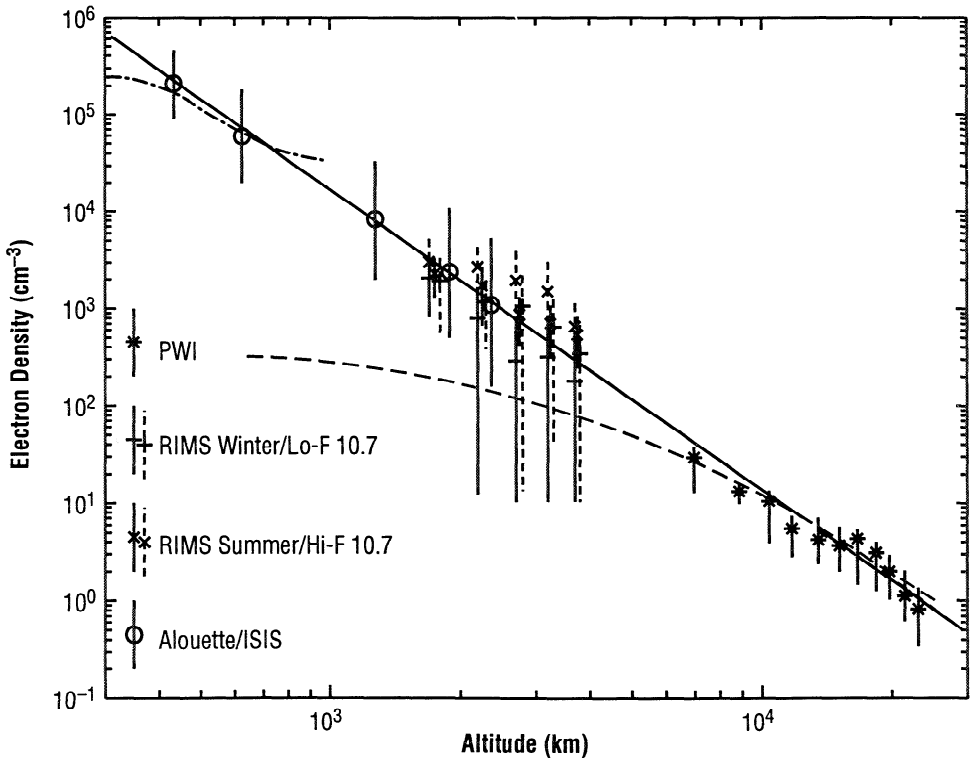

Figure 9. Average polar cap densities versus altitude are shown from DE 1/PWI (asterisk-solid line), from DE 1/RIMS in northern winter (plus-solid line), from DE 1/RIMS for low $F_{10.7}$ conditions (plus-dashed line), from DE 1/RIMS for northern summer (cross-solid line), from DE 1/RIMS for high $F_{10.7}$ conditions (cross-dashed line), and from the Alouette and ISIS spacecraft (circle-solid line) [*Persoon et al.*, 1983; *Chandler et al.*, 1991]. The linear line on this logarithmic-logarithmic display is a linear least squares fit of $\log_{10}$(density) versus the $\log_{10}$(altitude). It better represents the available statistical polar cap densities than the lower dashed curve from *Persoon et al.* [1983]. The upper dashed curve is from the IRI model to which the linear fit is matched to represent polar cap densities.

altitude instead of radial distance. Also included in this display are the densities from Alouette/ISIS topside sounding measurements presented by *Persoon et al.* [1983, Figure 12] and densities derived from the RIMS instrument on DE 1 by *Chandler et al.* [1991]. Chandler et al. presented individual ion densities for O^+, H^+, and He^+, which are summed here to obtain total density. RIMS-derived densities from *Chandler et al.* [1991] are shown for summer, winter, low $F_{10.7}$, and high $F_{10.7}$ conditions. For summer and high $F_{10.7}$ conditions the densities are somewhat higher than for winter and low $F_{10.7}$ conditions. For all conditions this display of density versus altitude reveals an approximately linear trend (on a logarithmic-logarithmic scale) that includes all three data sets. A linear least squares fit to the logarithms of density and altitude results in the expression

$$\log_{10}(n_e) = -3.09 \log_{10}(h) + 13.5 \quad , \tag{15}$$

where d is altitude in kilometers and n_e is density in cm^{-3}. The solid line in Figure 9 corresponds to the fit shown in equation (15). The dashed line in Figure 9 corresponds to the fit obtained by *Persoon et al.* [1983] for PWI-derived densities as a function of geocentric radial distance. We find these densities better ordered as a function of altitude, rather than a function of radial distance.

Not treated yet are the changes in density with seasonal and solar variations reported by *Chandler et al.* [1991]. The transition to ionospheric densities is also not yet included. In both cases, density increases with increasing illumination. Since only the observations of *Chandler et al.* [1991] (in Figure 9) include changes with varying conditions, it is not possible to directly model these variations with the current work. This is an area in which new POLAR spacecraft observations are available and will be used for improving the GCPM in the future. Since the IRI is already being used at lower latitudes and as a placeholder for better high-latitude ionospheric modeling, IRI will be used in the polar cap for the ionosphere. A sample of IRI-derived densities is shown in Figure 9 with a dash-dotted line. The dominant variation in the IRI-derived density profile at high latitudes is a variation in the height of the F_2 density peak. There are small changes in peak density and in the topside scale height. The approach that we use here to join the IRI and equation (15) is to adjust the constant term in equation (15), so that this equation intersects the IRI density profile at an altitude 200 km above the F_2 peak along any given field line. As the polar cap ionosphere "breaths" with changing conditions, the densities all along the field line will adjust upward or downward correspondingly, while preserving the power law density profile above the ionosphere.

8. Discussion

There are many things that the GCPM is not. It does not include, except on a statistical basis, features in cold plasma distribution that result from time-dependent effects; e.g., there are no sunward extended plasmaspheric tails. It also does not include all possible sources of data. Region-specific studies that make use of new sources of cold plasma density measurement can improve the characterizations provided by this first version of the GCPM. Assumptions and approximations have had to be made where no better information is available; e.g., the scale lengths over which transitions are made from trough to polar cap densities and the height along magnetic field lines where densities transition from ionospheric to plasmaspheric profiles. Enhanced auroral zone ionization is not yet explicitly represented, except insofar as the IRI represents these enhancements and the GCPM properly extends that effect to high altitudes. Ionospheric density profiles at high latitudes are provided by the IRI, even though it is not well defined at these latitudes.

The GCPM is at least two things: a framework and an approach for representing typical cold plasma properties throughout the volume of the inner magnetosphere. This property of the GCPM is intended to support its continued improvement. The GCPM provides a reference for typical core plasma densities throughout the inner magnetosphere. The densities returned by the GCPM are continuous in value and gradient. As discussed above, the relative densities of H^+, He^+, and O^+ (obtained for the plasmasphere) are also represented. The GCPM provides core plasma density as a function of solar magnetic coordinate position, geomagnetic activity (K_p), solar luminosity ($F_{10.7}$), average annual sunspot number, and time.

There is a great need in the science and engineering communities to obtain generalized descriptions of the magnetospheric environment. The GCPM is our attempt to provide a first global approximation of the typical properties of cold plasma in the inner magnetosphere. It is also our attempt to include many of the contributions made by the research community to generalize and model cold plasma densities in various magnetospheric regions. The intent is that the GCPM will serve as a framework upon which future advancements in empirical descriptions of regional or global thermal plasma properties can be incorporated.

Acknowledgments. The authors wish to acknowledge use of densities derived from the University of Iowa DE 1 PWI. C. W. Piker and J. D. Menietti have provided these data. D. Gallagher wishes to extend a special thanks to Richard Denton for many productive discussions during the development of this work. Work performed at the University of Iowa and at NASA Marshall Space Flight Center was supported by the NASA Office of Space Science. The work of R.H.C. has been partially supported under NCC8-65 and NAG5-4268.

Janet G. Luhmann thanks both of the referees for their assistance in evaluating this paper.

References

Angerami, J. J., and D. L. Carpenter, Whistler studies of the plasmapause in the magnetosphere, 2, Electron density and total tube content near the knee in magnetospheric ionization, *J. Geophys. Res.*, *71*, 711, 1966.

Binsack, J. H., Plasmapause observations with the M.I.T. experiment on IMP 2, *J. Geophys. Res.*, *72*, 5231, 1967.

Brace, L. H., and R. F. Theis, The behavior of the plasmapause at midlatitudes: Sis 1 Langmuir probe measurements, *J. Geophys. Res.*, *79*, 1871, 1974.

Bilitza, D., K. Rawer, L. Bossy, and T. Gulyaeva, International Reference Ionosphere—Past, present, and future, *Adv. Space Res.*, *13*, 3, 1993.

Booker, H. G., Fitting of multi-region ionospheric profiles of electron density by a single analytic function of height, *J. Atmos. Terr. Phys.*, *39*, 619, 1977.

Carpenter, D. L., Whistler studies of the plasmapause in the magnetosphere, 1, Temporal variations in the position of the knee and some evidence on plasma motions near the knee, *J. Geophys. Res.*, *71*, 693, 1966.

Carpenter, D. L., Whistler evidence of the dynamic behavior of the duskside bulge in the plasmasphere, *J. Geophys. Res.*, *75*, 3837, 1970.

Carpenter, D. L., and R. R. Anderson, An ISEE/whistler model of equatorial electron density in the magnetosphere, *J. Geophys. Res.*, *97*, 1097, 1992.

Carpenter, D. L., and R. L. Smith, Whistler measurements of electron density in the magnetosphere, *Rev. Geophys.*, *2*, 415, 1964.

Carpenter, D. L., B. L. Giles, C. R. Chappell, P. M. E. Decreau, R. R. Anderson, A. M. Persoon, A. J. Smith, Y. Corcuff, and P. Canu, Plasmasphere dynamics in the duskside bulge region: A new look at an old topic, *J. Geophys. Res.*, *98*, 19,243, 1993.

Chandler, M. O., J. H. Waite Jr, and T. E. Moore, Observations of polar ion outflows, *J. Geophys. Res.*, *96*, 1421, 1991.

Chappell, C. R., K. K. Harris, and G. W. Sharp, The morphology of the bulge region of the plasmasphere, *J. Geophys. Res.*, *75*, 3848, 1970.

Chappell, C. R., K. K. Harris, and G. W. Sharp, The dayside of the plasmasphere, *J. Geophys. Res.*, *76*, 7632, 1971.

Comfort, R. H., Auroral oval kinematics program, *NASA CR-61373*, NASA, Washington, D.C., Jan. 1972.

Comfort, R. H., I. T. Newberry, and C. R. Chappell, Preliminary statistical survey of plasmaspheric ion properties from observations by DE 1/RIMS, in *Modeling Magnetospheric Plasma, Geophys. Monogr. Ser.*, Vol. 44, edited by T. E. Moore and J. H. Waite Jr., p. 107, AGU, Washington, D.C., 1988.

Craven, P. D., R. H. Comfort, P. G. Richards, and J. Grebowsky, Comparisons of modeled N^+, O^+, H^+, and He^+ in the midlatitude ionosphere with mean densities and temperatures from Atmospheric Explorer, *J. Geophys. Res.*, *100*, 257, 1995.

Craven, P. D., D. L. Gallagher, and R. H. Comfort, Relative concentration of He^+ in the inner magnetosphere as observed by the DE 1 retarding ion mass spectrometer, *J. Geophys. Res.*, *102*, 2279, 1997.

Decreau, P. M. E., B. Beghin, and M. Parrot, Global characteristics of the cold plasma in the equatorial plasmapause region as deduced from the GEOS 1 mutual impedance probe, *J. Geophys. Res.*, *87*, 695, 1982.

Decreau, P. M. E., D. Carpenter, C. R. Chappell, R. H. Comfort, J. Green, R. C. Olsen, and J. H. Waite Jr., Latitudinal plasma distribution in the dusk plasmaspheric bulge: Refilling phase and quasi-equilibrium state, *J. Geophys. Res.*, *91*, 6929, 1986.

Feldstein, Y. I., and G. V. Starkov, Dynamics of auroral belt and polar geomagnetic disturbances, *Planet. Space Sci.*, *15*, 209, 1967.

Feldstein, Y. I., and G. V. Starkov, The polar auroral band during magnetic disturbances (in Russian), in *Auroras*, Vol. 17, edited by S. I. Isayev and Y. I. Feldstein, 1968. (English translation, *NASA TT F–637*, NASA, Washington, D.C., June 1971.)

Freeman, R. M., Langmuir probe studies of low energy magnetospheric plasma, Ph.D. thesis, Univ. of London, London, 1973.

Gallagher, D. L., and P. D. Craven, Initial development of a new empirical model of the Earth's inner magnetosphere for density, temperature, and composition, in *Modeling Magnetospheric Plasma, Geophys. Monogr. Ser.*, Vol. 44, edited by T. E. Moore and J. H. Waite Jr., p. 61, AGU, Washington, D.C., 1988.

Gallagher, D. L., P. D. Craven, and R. H. Comfort, An empirical model of the Earth's plasmasphere, *Adv. Space Res.*, *8*, 15, 1988.

Gallagher, D. L., P. D. Craven, R. H. Comfort, and T. E. Moore, On the azimuthal variation of core plasma in the equatorial magnetosphere, *J. Geophys. Res.*, *100*, 23,597, 1995. (Correction, *J. Geophys. Res.*, *102*, 2437, 1997).

Gallagher, D. L., P. D. Craven, and R. H. Comfort, A simple model of magnetospheric trough total density, *J. Geophys. Res.*, *103*, 9293, 1998.

Gringauz, K. I., and V. V. Bezrukikh, Asymmetry of the Earth's plasmasphere in the direction noon-midnight from Prognoz and Prognoz-2 data, *J. Atmos. Terr. Phys.*, *38*, 1071, 1976.

Gringauz, K. I., V. V. Bezrukikh, V. D. Ozerov, and R. Ye. Rybchinsky, A study of interplanetary ionized gas, energetic electrons, and corpuscular solar emissions, using three-electrode charge-particle traps set up on the second Soviet cosmic rocket Luna 2 (in Russian), *Dokl. Akad. Nauk USSR*, *131*, 1301, 1960a. (English translation, *Soviet Phys. Doklady*, *5*, 361, 1960.)

Gringauz, K. I., V. G. Kurt, V. I. Moroz, and I. S. Shklovsky, Results of observations of charged particles observed out to 100,000 km with the aid of charged particle traps on Soviet space probes, *Astron. Zhur.*, *37*, 716, 1960b. (English translation, *Soviet Astron. Engl. Transl.*, *4*, 680, 1961.)

Higel, B., and W. Lei, Electron density and plasmapause characteristics at 6.6 R_E: A statistical study of the GEOS 2 relaxation sounder data, *J. Geophys. Res.*, *89*, 1583, 1984.

Horwitz, J. L., R. H. Comfort, and C. R. Chappell, A statistical characterization of plasmasphere density structure and boundary locations, *J. Geophys. Res.*, *95*, 7937, 1990.

Knott, K., R. Grard, and A. Pedersen, Radial discontinuities in low-energy magnetospheric plasma observed on GEOS-1, paper presented at Magnetospheric Boundary Layers Conference, European Space Agency, ESA SP-148, Alpbach, Austria, pp. 75–79, June 11–15, 1979.

Maynard, N. C., and J. M. Grebowsky, The plasmapause revisited, *J. Geophys. Res.*, *82*, 1591, 1977.

Moldwin, M. B., M. F. Thomsen, S. J. Bame, D. J. McComas, and K. R. Moore, An examination of the structure and dynamics of the outer plasmasphere using multiple geosynchronous satellites, *J. Geophys. Res.*, *99*, 11,475, 1994.

Nishida, A., Formation of plasmapause, or magnetospheric plasma knee, by the combined action of magnetospheric convection and plasma escape from the tail, *J. Geophys. Res.*, *71*, 5669, 1966.

Olsen, R. C., S. D. Shawhan, D. L. Gallagher, J. L. Green, C. R. Chappell, and R. R. Anderson, Plasma observations at the Earth's magnetic equator, *J. Geophys. Res.*, *92*, 2385, 1987.

Park, C. G., D. L. Carpenter, and D. B. Wiggin, Electron density in the plasmasphere: Whistler data on solar cycle, annual, and diurnal variations, *J. Geophys. Res.*, *83*, 3137, 1978.

Persoon, A. M., D. A. Gurnett, and S. D. Shawhan, Polar cap electron densities from DE 1 plasma wave observations, *J. Geophys. Res.*, *88*, 10,123, 1983.

Pope, J. H., An estimate of electron densities in the exosphere by means of nose whistlers, *J. Geophys. Res.*, *66*, 67, 1961.

Rawer, K., New description of the electron density profile, *Adv. Space Res.*, *4*, 11, 1984.

Richards, P. G., D. G. Torr, and K. L. Miller, O^+, H^+, and He^+ densities from the 200–1600 km altitude ionosphere at Arecibo: A comparison of theory and measurement, in *Modeling Magnetospheric Plasma Processes, Geophys. Monograph Ser.*, Vol. 62, p. 167, AGU, Washington, D.C., 1991.

Richards, P. G., J. A. Fennelly, and G. G. Torr, EUVAC: A solar EUV flux model for aeronomic calculations, *J. Geophys. Res.*, *99*, 8981, 1994.

Rycroft, M. J., A review of in situ observations of the plasmapause, *Ann. Geophys.*, *31*, 2, 1975.

Rycroft, M. J., and I. R. Jones, Modeling the plasmasphere for the international reference ionosphere, *Adv. Space Res.*, *5*, 21, 1985.

Rycroft, M. J., and I. R. Jones, A suggested model for the IRI plasmaspheric distribution, *Adv. Space Res.*, *7*, 13, 1987.

Rycroft, M. J., and J. O. Thomas, The magnetospheric plasmapause and the electron density trough at the Alouette 1 orbit, *Planet. Space Sci.*, *18*, 65, 1970.

Smith, R. L., Properties of the outer ionosphere deduced from nose whistler, *J. Geophys. Res.*, *66*, 3709, 1961.

Storey, L. R. O., An investigation of whistling atmospherics, *Phil. Trans. of the Royal Soc.* (London) A, *246*, 113, 1953.

Taylor, H. A., Jr., H. C. Brinton, and C. R. Smith, Positive ion composition in the magnetosphere obtained from the Ogo-A satellite, *J. Geophys. Res.*, *70*, 5769, 1965.

Taylor, H. A., H. C. Brinton, and A. R. Deshmukh, Observations of irregular structure in thermal ion distributions in the duskside magnetosphere, *J. Geophys. Res.*, *75*, 2481, 1970.

Torr, M. R., D. G. Torr, P. G. Richards, and S. P. Yung, Mid- and low-latitude model of thermosphere emissions, 1, $O^+(^2P)$ 7320 Å and $N_2(^2P)$ 3371 Å, *J. Geophys. Res.*, *95*, 147, 1990.

R. H. Comfort, Center for Space Plasma and Aeronomic Research, University of Alabama in Huntsville, Huntsville, AL 35807.

P. D. Craven and D. L. Gallagher, SD50, Space Science Department, Marshall Space Flight Center, AL 35812. (Dennis.Gallagher@msfc.nasa.gov)

(Received July 2, 1999; revised December 29, 1999;
accepted December 29, 1999.)